

Li/Fe modified $\text{Zn}_{0.3}\text{Ni}_{0.7}\text{O}$ NTC thermistors with adjustable resistivities and temperature sensitivity

Xiang Sun¹ · Zhicheng Li^{1,2} · Weiyi Fu¹ · Shiyuan Chen¹ · Hong Zhang^{1,2}

Received: 10 July 2017 / Accepted: 26 September 2017 / Published online: 13 October 2017
© Springer Science+Business Media, LLC 2017

Abstract Li/Fe modified $\text{Zn}_{0.3}\text{Ni}_{0.7}\text{O}$, $(\text{Zn}_{0.3}\text{Ni}_{0.7})_{1-x-y}\text{Li}_x\text{Fe}_y\text{O}$ ($x=0-0.06$, $y=0-0.04$), were synthesized by a wet chemical synthesis methods and sintered by the traditional ceramic sintering technology. The phase component and related electrical properties of the ceramics were investigated. The analysis of X-ray diffraction indicates that all the prepared ceramics have a cubic crystalline structure. The resistance-temperature feature exhibits a typical effect of negative temperature coefficient (NTC) of resistivity in a temperature range from 25 to 250 °C. The ceramics have room-temperature resistivities ranging from 26.6 Ω cm to 102.8 MΩ cm and thermal-sensitivity constants from 2444 to 8378 K by changing the concentrations of Li and Fe. The complex impedance analysis reveals that both grain effect and grain boundary effect contribute collectively to the NTC feature of the ceramics. The possible conduction models were proposed to combine with electron-hopping conduction and band conduction.

1 Introduction

Negative temperature coefficient (NTC) thermistors are widely applied in the fields of automotive, house appliances and aerospace as the key elements for suppression of temperature measurements and controlling, in-rush current, etc., due to the unique temperature sensitivity, fast response and

low cost. Transition-metal compounds with the spinel structure, such as Mn–Ni–O, Ni–Fe–O, Mn–Fe–O, Ni–Cu–Mn–O and Mn–Co–Ni–O system [1–5], are always the common NTC thermistors. However, the structural relaxation occurred in these kinds of NTC compounds restricts their applications at temperatures below 200 °C. For improving the electrical property and ageing characteristic, numerous work have been tried by the way of cation doping and microstructure modification, etc. Meanwhile, in the spinel manganite ceramics, a polaron hopping model is generally accepted as the main conduction mechanism, where the hopping conduction takes place between the valence-variable ions such as $\text{Mn}^{3+}/\text{Mn}^{4+}$ cations locating on the octahedral sites [6, 7]. The exact oxidation states of the Mn-cations in the spinel obviously rely on the oxygen partial pressure and the sintering temperature, therefore, a minor change of the sintering condition might lead to a considerably different $\text{Mn}^{3+}/\text{Mn}^{4+}$ concentration and affect the room-temperature resistivity (ρ_{25}) [8, 9]. For the practical applications, it is quite key to tap the NTC ceramics system with the adjustable resistivity, appropriate thermal-sensitivity constant B value. So a series of new systems of NTC ceramics have been developed, e.g., inverse spinel-type $\text{Zn}_7\text{Sb}_2\text{O}_{12}$, pyrochlore type $\text{Bi}_3\text{Zn}_2\text{Sb}_3\text{O}_{14}$ compounds, and even modified simple oxides such as SnO_2 , CuO and NiO [10–15].

Compared to the spinel thermistors, the distinct advantages of the semiconducting oxides for the NTC applications are that the ρ_{25} can be effectively adjusted by element doping and the related B value can be modified by suitable element substitution [13–17]. NiO is one typical semiconductive material with the band gap of 3.6–4.0 eV and has aroused numerous interests for the various applications such as gas-sensors, catalyst, dielectric, and even the electrodes for supercapacitors and lithium-ion batteries [18–20]. Zinc oxide (ZnO), as a semiconductor with the band gap of about

✉ Hong Zhang
hzhang@csu.edu.cn

¹ School of Materials Science and Engineering, Central South University, Changsha 410083, China

² State Key Laboratory of Powder Metallurgy, Central South University, Changsha 410083, China

3.37 eV, has also attracted much attentions for several decades due to its potential applications in light emitting diodes, solar cells, transparent conductive films, varistors, biosensors, etc. [21, 22]. Many researches on Zn–Ni–O system materials have conducted and mainly focused on the crystalline structure, optical properties and magnetic properties, etc. [23–25]. $Zn_{1-x}Ni_xO$ system ceramics have been recently reported to show the NTC characteristic with high $B_{25/85}$ values [26].

It should be quite interesting of a compound system, to meet various applications, that both ρ_{25} and $B_{25/85}$ can be adjusted in a large range by doping and/or substituting of a small quantity of additives. In this work, the Li/Fe modified $Zn_{0.3}Ni_{0.7}O$ ceramics were investigated, and the results show that the prepared ceramics have the typical NTC effect, the ρ_{25} and $B_{25/85}$ can be controlled effectively by changing the concentrations of Li and Fe ions. The related electrical properties and conduction mechanisms were investigated in this work.

2 Experimental procedures

Li/Fe modified $Zn_{0.3}Ni_{0.7}O$, $(Zn_{0.3}Ni_{0.7})_{1-x-y}Li_xFe_yO$ ($x=0, 0.005, 0.1, 0.015, 0.02, 0.03, 0.04, 0.05$ and 0.06 ; $y=0, 0.01, 0.015, 0.02, 0.025, 0.03$ and 0.04), powders were prepared by a wet chemical process with polyvinyl alcohol (PVA) as a polymeric carrier. As the starting materials, basic nickel carbonate ($NiCO_3 \cdot 2Ni(OH)_2 \cdot 4H_2O$), zinc oxide (ZnO), lithium carbonate (Li_2CO_3), ferric citrate ($FeC_6H_5O_7 \cdot nH_2O$) were selected. These raw materials were weighed, respectively, according to the formula of $(Zn_{0.3}Ni_{0.7})_{1-x-y}Li_xFe_yO$ in each batch. $NiCO_3 \cdot 2Ni(OH)_2 \cdot 4H_2O$, ZnO and Li_2CO_3 were dissolved into nitric acid solution (about 5 vol% HNO_3 in distilled H_2O), $FeC_6H_5O_7 \cdot 5H_2O$ was dissolved into the hot distilled water. Then the solutions were mixed together. A proper amount of PVA, as the polymeric carrier for the effective preparation of mixed oxides, was added into the solution. The mixed solution was heated and dried under magnetic stirring to get the precursor. The precursor was calcined at $1000^\circ C$ for 3 h, and then were pressed into pellets in 12 mm in diameter and about 3 mm in thickness. The obtained pellets were sintered at $1300^\circ C$ in air for 2 h. The surfaces of sintered pellets (ceramics) were ground and polished to the thickness of about 2 mm, and the electrodes were made on both opposite sides with silver paste by being heated at $600^\circ C$ for about 5 min.

The crystalline structure and phase component of the as-sintered ceramics were measured by X-ray diffraction (XRD, Rigaku D/max 2,500, Japan) with $Cu K_\alpha$ radiation and λ of 0.154056 nm. The ceramic microstructures were investigated with a scanning electron microscope (SEM, FEI Quanta200). For SEM observation, the ceramics were

broken into pieces and the related fracture surface was observed. The valence state and element content were investigated by X-ray photoelectron spectroscopy (XPS, K-alpha 1063, UK). The temperature dependence of resistance ($R-T$) of the samples was tested in the temperature range from 25 to $250^\circ C$ by an $R-T$ measurement system (ZWX-C, China). Taken account of the size of the sample, the resistivity ρ was calculated by Ohm's law of $\rho = RW/h$, where W is the electrode area, h is the thickness, and R is the resistance of the sample. The alternating current (AC) impedance measurements were performed at temperatures from 30 to $200^\circ C$ by an electrochemistry test system (Gamry Reference 600, USA) to analyze the conduction characteristic of the ceramics, the test frequency ranges from 1 Hz to 1 MHz.

3 Results and discussion

3.1 Phase and microstructure

Figure 1 shows the XRD patterns of the as-sintered ceramics of pure $Zn_{0.3}Ni_{0.7}O$, $(Zn_{0.3}Ni_{0.7})_{0.97}Li_{0.03}O$, $(Zn_{0.3}Ni_{0.7})_{0.955}Li_{0.03}Fe_{0.015}O$. All the XRD patterns can be indexed as the cubic phase with a space group of $Fm\bar{3}m$ (225) (referred by the PDF no. 75-0272). These indicate that the Li- and Fe- ions substituted into the $Zn_{0.3}Ni_{0.7}O$ lattice. By being refined with the Jade 6.0 + pdf2004 program, the lattice parameters are 0.4215, 0.4218 and 0.4206 nm for $Zn_{0.3}Ni_{0.7}O$, $(Zn_{0.3}Ni_{0.7})_{0.97}Li_{0.03}O$, $(Zn_{0.3}Ni_{0.7})_{0.955}Li_{0.03}Fe_{0.015}O$, respectively. The lattice parameter difference might result from the formation of the lattice vacancies and/or the solid solution for the Li- and Fe- ions substituted into the $Zn_{0.3}Ni_{0.7}O$ lattice. If the oxygen pressure was not so high during the ceramics sintering,

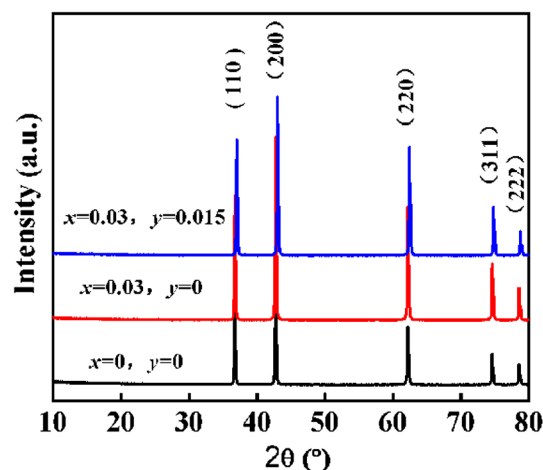


Fig. 1 XRD patterns of the as-sintered $(Zn_{0.3}Ni_{0.7})_{1-x-y}Li_xFe_yO$ ceramics for different substitution concentrations of Li- and Fe-ions

oxygen vacancies might formed in the $Zn_{0.3}Ni_{0.7}O$ ceramics. So the lattice parameter may not change obviously when Li-ion substituted, although the Li-substitution can induced the formation of oxygen vacancy for the $Zn_{0.3}Ni_{0.7}O$ itself might have oxygen vacancies and the radius of Li^+ (0.076 nm) is slightly larger than those of Zn^{2+} (0.074 nm) and Ni^{2+} (0.069 nm). While, the Fe^{3+} ion (0.065 nm) is smaller than those of Zn^{2+} and Ni^{2+} . When the Fe ions substituted into the crystal lattice, resulted in the decreasing of lattice parameter.

The SEM micrograph obtained from the section of the as-sintered $(Zn_{0.3}Ni_{0.7})_{0.955}Li_{0.03}Fe_{0.015}O$ ceramic is shown in Fig. 2. The morphology of the fracture surface shows a polycrystalline characteristic with the mean grain size about 5 μm . The grains connected closely each other, although some small pores in the ceramic. Some pores located inside the grains, might result from the quick temperature increasing during the sintering process and gas could not volatilize sufficiently from the pellet.

In order to distinguish the possible valences of Ni-cations and the effect of Fe-substitution in the valence change in the ceramics, XPS analysis of the ceramics of $(Zn_{0.3}Ni_{0.7})_{0.97-y}Li_{0.03}Fe_yO$ ceramics with and without Fe-substitution ($y=0.015$ and $y=0.0$) were performed as shown in Fig. 3. One can see from the XPS spectrum of $(Zn_{0.3}Ni_{0.7})_{0.97}Li_{0.03}O$ ceramic, the Ni $2p_{3/2}$ peak and its satellite at binding energies ~ 853.9 and 860.8 eV, respectively, and the Ni $2p_{1/2}$ main peak and its satellite peak locate at 872.0 and 880.1 eV. Whereas, the Fe-doped $(Zn_{0.3}Ni_{0.7})_{0.97}Li_{0.03}O$ ceramic shows an about 0.6 eV shift towards higher binding energy, comparing to the $(Zn_{0.3}Ni_{0.7})_{0.97}Li_{0.03}O$ sample. These peaks are in a good agreement with those reported by Gokul et al. [27], indicating that two kinds of Ni-ions (Ni^{3+} and Ni^{2+}) exist in the $(Zn_{0.3}Ni_{0.7})_{1-x-y}Li_xFe_yO$ ceramics.

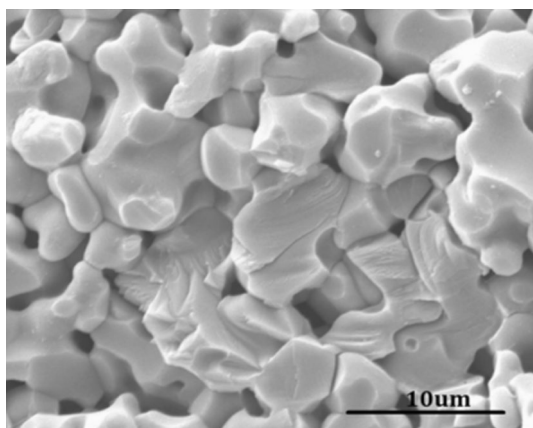


Fig. 2 SEM micrograph of the as-sintered $(Zn_{0.3}Ni_{0.7})_{0.955}Li_{0.03}Fe_{0.015}O$ ceramic

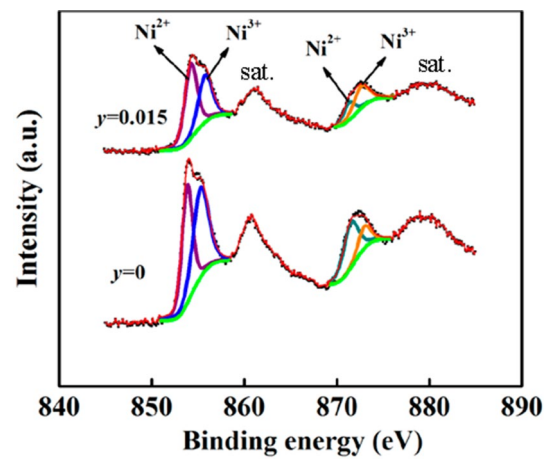


Fig. 3 XPS spectra of the Ni 2p in the $(Zn_{0.3}Ni_{0.7})_{0.97-y}Li_{0.03}Fe_yO$ ceramics with $y=0$ and 0.015

3.2 Electrical properties

As well known, the conductivity of a semiconductor can be effectively adjusted by doping with suitable dopants [14–19, 24, 26]. Li-doped $Zn_{0.3}Ni_{0.7}O$ ceramics, $(Zn_{0.3}Ni_{0.7})_{1-x}Li_xO$, were prepared to study the influence of Li-content on the electrical properties, and then the effect of Fe-concentration in the electrical properties and temperature sensitivity of $(Zn_{0.3}Ni_{0.7})_{1-x-y}Li_xFe_yO$ ceramics were further investigated in details in this work. The room temperature resistivities of the $(Zn_{0.3}Ni_{0.7})_{1-x}Li_xO$ ceramics are 406.3, 238, 188.4, 116.4, 38.2, 26.6, 116.3, 151.8 and 611.4 Ωcm for the $x=0, 0.005, 0.01, 0.015, 0.02, 0.03, 0.04, 0.05$ and 0.06 , respectively. The results indicate that acceptor Li^+ ion is a useful semiconducting dopant for $Zn_{0.3}Ni_{0.7}O$ ceramics.

Figure 4a shows the Arrhenius plots of the temperature dependence of resistivity ($\ln\rho-1000/T$) of the $(Zn_{0.3}Ni_{0.7})_{0.97-y}Li_{0.03}Fe_yO$ ceramics with various Fe contents. All the ceramics show the NTC effect. When $y \leq 0.03$, the $\ln\rho-1000/T$ relationship is nearly linear in the testing temperature range from 25 to 250 $^{\circ}C$. But when $y \geq 0.04$, the $\ln\rho-1000/T$ lost the monotonously linear relationship, which might resulted from the formation of second phases as the Fe-content increase. The linear resistivity-temperature relationship could be approximately expressed by the Arrhenius law as shown in Eq. (1).

$$\rho_T = A \exp \frac{E_a}{kT} \tag{1}$$

where, ρ_T is the resistivity at temperature T (T , in Kelvin), k is the Boltzmann constant, A is a constant related to the material characteristic, E_a is the activation energy of conduction. The NTC thermal sensitivity constant ($B_{25/85} = E_a/k$) is always calculated by using the data measured at 298 K (25 $^{\circ}C$) and 358 K (85 $^{\circ}C$) by Eq. (2).

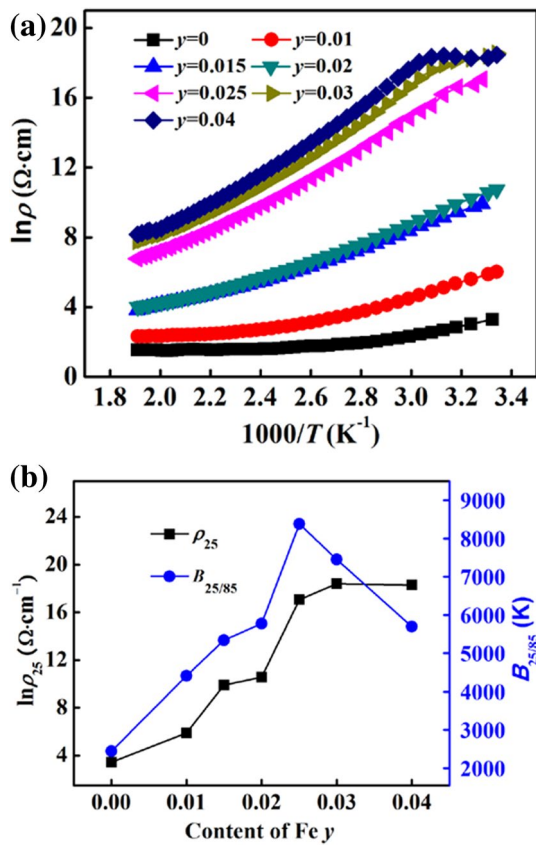


Fig. 4 Electrical properties of the ceramics, **a** temperature dependence of resistivity of the $(\text{Zn}_{0.3}\text{Ni}_{0.7})_{0.97-y}\text{Li}_{0.03}\text{Fe}_y\text{O}$ ceramics ($y=0, 0.01, 0.015, 0.02, 0.025, 0.03, 0.04$) in Arrhenius plots, **b** Fe-concentration dependence of room-temperature resistivities ρ_{25} and thermal sensitivity constant $B_{25/85}$

$$B_{25/85} = \frac{\ln \rho_{25} - \ln \rho_{85}}{1/T_{25} - 1/T_{85}} \quad (2)$$

where, ρ_{25} and ρ_{85} are the resistivities at 298 K (25 °C) and 358 K (85 °C), respectively.

The Fe-concentration dependence of ρ_{25} and $B_{25/85}$ of the $(\text{Zn}_{0.3}\text{Ni}_{0.7})_{0.97-y}\text{Li}_{0.03}\text{Fe}_y\text{O}$ ceramics are shown in Fig. 4b. For the concentrations y are 0, 0.01, 0.015, 0.02, 0.025, 0.03 and 0.04, the ρ_{25} are 26.6, 4.096×10^2 , 1.989×10^4 , 4.642×10^4 , 2.588×10^7 , 1.126×10^8 and $1.028 \times 10^8 \Omega \cdot \text{cm}$, respectively, and the related thermal constant B values are 2444, 4413, 5345, 5779, 8378, 7455 and 5702 K, respectively. It is worthy of attention that ρ_{25} and $B_{25/85}$ of the Li-doped $\text{Zn}_{0.3}\text{Ni}_{0.7}\text{O}$ based ceramics are effectively tunable by the way of changing the content of Fe. For the commercial applications, 2000–6000 K of the B values are required. The adjustable ρ_{25} and $B_{25/85}$ of the $(\text{Zn}_{0.3}\text{Ni}_{0.7})_{1-x-y}\text{Li}_x\text{Fe}_y\text{O}$ ceramics indicate that these system have great potential for practical applications.

According to the measurement and analysis of the $(\text{Zn}_{0.3}\text{Ni}_{0.7})_{1-x-y}\text{Li}_x\text{Fe}_y\text{O}$ ceramics as discussed above.

When the concentration y is small, Fe-ions could entirely substitute into the $\text{Zn}_{0.3}\text{Ni}_{0.7}\text{O}$ lattice, as confirmed by the XRD analysis above. The existence of Fe^{3+} might induce the point defects such as lattice distortion for the different radii between the Fe-ion and Ni(Zn)-ions, accompanying with higher lattice barrier, resulting in the rise of ρ_{25} and $B_{25/85}$. On the other hand, second phase or impurities might occur when the y increase, and located at the grain shells or grain boundaries, although it could not be evaluated by the XRD measurement in Fig. 1 for the limit quantity. This could also lead to the rise of ρ_{25} and $B_{25/85}$ in the ceramics.

3.3 Impedance and electric modulus

In order to bring light for the conduction characteristic of the ceramics, AC impedance spectroscopy was employed in this work. In general, a complex impedance spectrum of an ideal polycrystalline ceramics is composed of three semicircles, which represent grain effect, grain boundary effect and the electrode polarization effect, respectively [15–18, 28]. The impedance data $Z(\omega)$ is usually plotted in the Cole–Cole plane as Eq. (3).

$$Z(\omega) = Z' + jZ'' \quad (3)$$

where, ω is the angular frequency, Z' and Z'' are respectively the real and imaginary parts of the complex impedance, and $j = \sqrt{-1}$ is the imaginary factor. A series of complex impedance spectra of a $(\text{Zn}_{0.3}\text{Ni}_{0.7})_{0.955}\text{Li}_{0.03}\text{Fe}_{0.015}\text{O}$ ceramic, measured at various temperatures, are shown in Fig. 5a, b. Due to the limited frequency of the measurement system, only one arc or part arc can be directly observed at various temperatures. An equivalent circuit is applied to fit the measured impedance data (see the inset in Fig. 5a). Where, R_1 and R_2 represent respectively the resistances from grain effect and grain boundary effect, $CPE1$ and $CPE2$ are the related constant phase elements due to interior structure inhomogeneity or some other uncertain defects such as impurity. The fitted results reveal that each plot contains two suppressed semicircles related to the grain effect at higher frequency region and grain boundary effect at lower frequency region. This indicates that those two semicircles overlapped partially each other.

Figure 5c shows the temperature dependence of R_g and R_{gb} . One can see that $\ln R_{gb}$ is higher than that of $\ln R_g$ at each temperature, indicating that the main contribution comes from grain boundary effect to the ceramic resistance. Meanwhile, all of $\ln R_{gb}$, $\ln R_g$ and $\ln(R_g + R_{gb})$ present the obvious characteristic of NTC effect.

Figure 6a displays the frequency dependence of imaginary part of impedance (Z'') for the $(\text{Zn}_{0.3}\text{Ni}_{0.7})_{0.955}\text{Li}_{0.03}\text{Fe}_{0.015}\text{O}$ ceramic at various temperatures. The inset plot shows the magnified drawing. Regardless of all experimental temperatures, the value of Z'' tends to zero at low frequency,

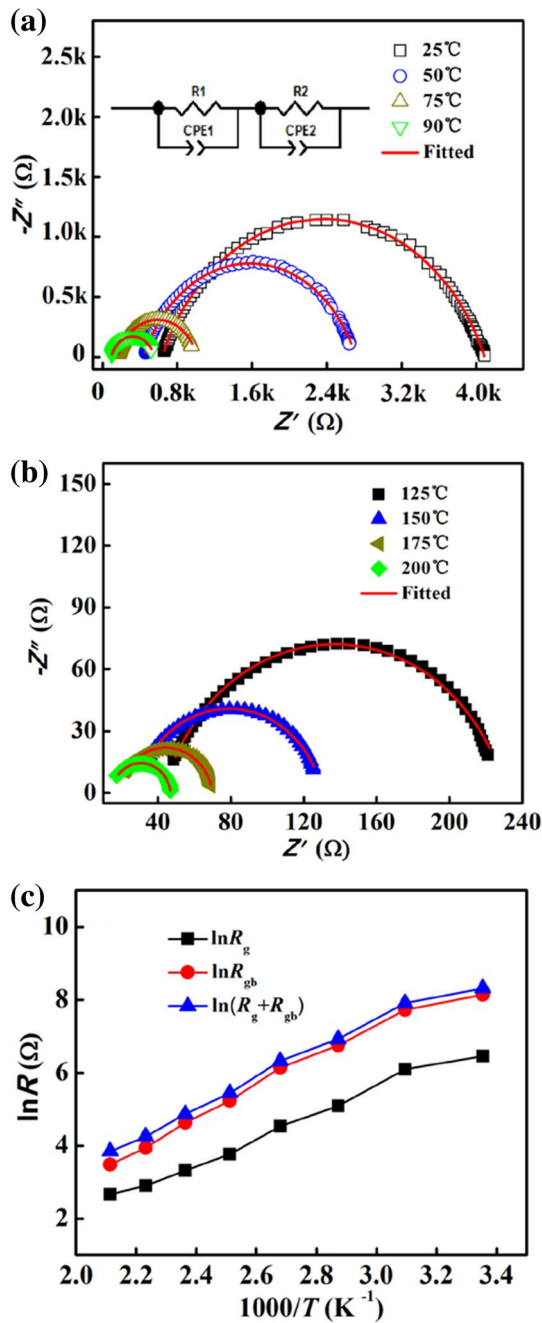


Fig. 5 Analysis of the temperature dependence of impedance spectra of $(\text{Zn}_{0.3}\text{Ni}_{0.7})_{0.955}\text{Li}_{0.03}\text{Fe}_{0.015}\text{O}$ ceramic at various temperatures, **a** at 25, 50, 75 and 100 °C, the inset is an equivalent circuit for fitting the impedance data, **b** at 125, 150, 175 and 200 °C, **c** temperature dependence of impedances from grain effect (R_g), grain boundary effect (R_{gb}) and total resistance (R_g+R_{gb})

indicating a weak electrode polarization. Each plot contains only one peak, the peak shifts to higher frequency region and further broadens with temperature rise. This indicates a temperature-dependent electrical relaxation behavior in the ceramics, for the existence of immobile species at lower

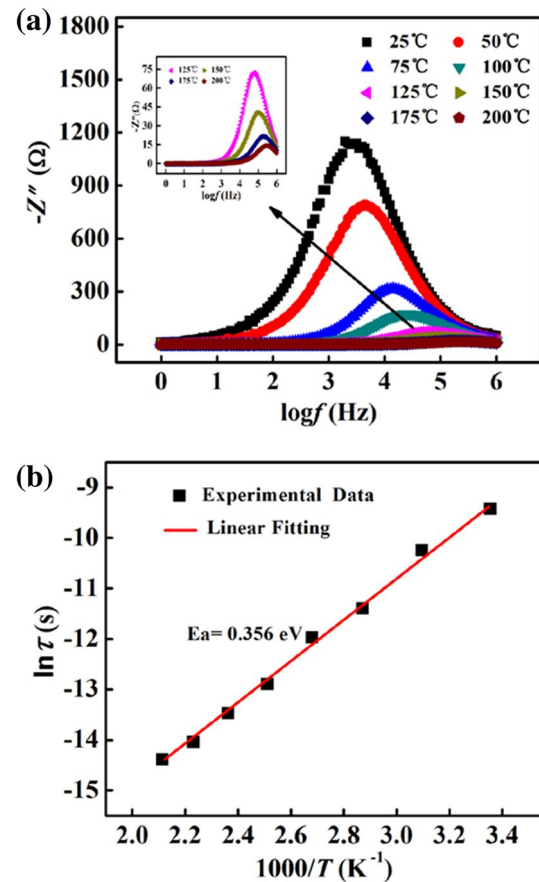


Fig. 6 Analysis of the imaginary impedance part Z'' of $(\text{Zn}_{0.3}\text{Ni}_{0.7})_{0.955}\text{Li}_{0.03}\text{Fe}_{0.015}\text{O}$ ceramic, **a** plots for frequency dependent of Z'' at various temperatures, **b** variation of relaxation time τ with inverse of absolute temperature

temperatures and defects at higher temperatures. The relationship between peak height Z'' and the resistance can be described by Eq. (4) [29].

$$Z'' = R \left[\frac{\omega\tau}{1 + (\omega\tau)^2} \right] \tag{4}$$

where, R is resistance, $\omega = 2\pi f$ is angular frequency, τ is relaxation time. As the result, the relaxation time decreases with rise in temperature, indicating the presence of thermally activated conduction. In a relaxation system, the impedance loss spectra can be used to evaluate the relaxation time τ of the electrical phenomena according to the relationship in Eq. (5) [30].

$$\tau = \frac{1}{\omega} = \frac{1}{2\pi f_{\max}} \tag{5}$$

where, f_{\max} is characteristic frequency maximum known as relaxation frequency which depends on temperature. Variation of corresponding values τ with inverse of absolute

temperature is illustrated in Fig. 6b. It is shown that the values of τ increases with the rise in temperature, suggesting the typical temperature-dependent electrical relaxation phenomena in the $(\text{Zn}_{0.3}\text{Ni}_{0.7})_{1-x-y}\text{Li}_x\text{Fe}_y\text{O}$ ceramics.

To reveal the transport characteristic of charge carriers in the $(\text{Zn}_{0.3}\text{Ni}_{0.7})_{1-x-y}\text{Li}_x\text{Fe}_y\text{O}$ ceramics, normalized imaginary impedance (Z''/Z''_{max}) and electrical modulus (M''/M''_{max}) of $(\text{Zn}_{0.3}\text{Ni}_{0.7})_{0.955}\text{Li}_{0.03}\text{Fe}_{0.015}\text{O}$ at various temperatures were analyzed. The temperature dependence of normalized values are shown in Figs. 7a, b. At each temperature, the plots of M''/M''_{max} decreases to zero with the frequency decreases in the low frequency region, implying that a negligible or absent electrode polarization phenomenon. The peak frequencies mismatch with each other between the $Z''/Z''_{\text{max}} - \log\omega$ and $M''/M''_{\text{max}} - \log\omega$ plots at each temperature. These indicate the presence of localized conduction such as a hopping conduction model, and is different from the ideal Debye type of conductivity relaxation in which the Z''_{max} and M''_{max} peak frequencies are compatible.

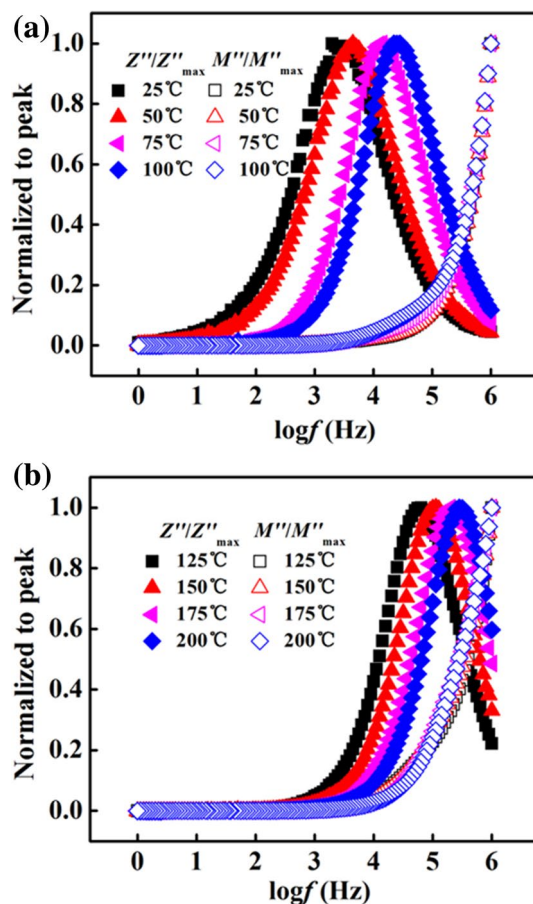


Fig. 7 Comparison plots of frequency dependent of normalized imaginary impedance (Z''/Z''_{max}) and electrical modulus (M''/M''_{max}) of $(\text{Zn}_{0.3}\text{Ni}_{0.7})_{0.955}\text{Li}_{0.03}\text{Fe}_{0.015}\text{O}$ ceramic at various temperatures, **a** 25, 50, 75 and 100 °C, **b** 125, 150, 175 and 200 °C

In the meantime, the complex impedance $Z(\omega)$ can be converted into a complex admittance $Y(\omega)$ by using the relationship of $Y(\omega) = 1/Z(\omega)$. The real part admittance can be obtained by $Y'(\omega) = Z'/|Z|^2$. Taken account of the size of the sample, the real part conductivity of $\sigma'(\omega)$ can be described by Eq. (6) $\sigma'(\omega)$ based on the Jonscher's universal response law [31].

$$\sigma'(\omega) = \sigma'(0) + A\omega^S \quad (6)$$

where, $\sigma'(\omega)$ is the real part conductivity depending on frequency, ω is the angular frequency, $\sigma'(0)$ is the DC conductivity which can be extracted from the value of $\sigma'(\omega)$ when ω tends to zero, A is thermally activation constant depending on temperature, S is the power exponent which is temperature and material dependent. S is considered to be < 1 for hopping conduction [32]. Figure 8 shows the relationship between $\log[\sigma'(\omega) - \sigma'(0)]$ and $\log\omega$ of the $(\text{Zn}_{0.3}\text{Ni}_{0.7})_{0.955}\text{Li}_{0.03}\text{Fe}_{0.015}\text{O}$ ceramic from 25 to 200 °C. Due to the limited frequency and resolution of the measurement apparatus, the complex impedance could not be measured at higher temperature. It is convenient to get the values of A and S by reading the intercept and slope of the fitted plots. The S values are 0.496, 0.645, 0.848, 0.936, 0.984, 1.031, 1.086 and 1.196 at temperatures of 25, 50, 75, 100, 125, 150, 175 and 200 °C, respectively. In lower temperature region (≤ 125 °C), the S values are less than 1, confirming the dominant contribution from the hopping conduction. While, the S values are more than 1 at higher temperature region (≥ 150 °C), indicating the hopping conduction is not the unique model for charge carriers transition. In other words, band conduction should also play an important role to the conduction mechanisms at higher temperature region, and will be discussed in details in next section.

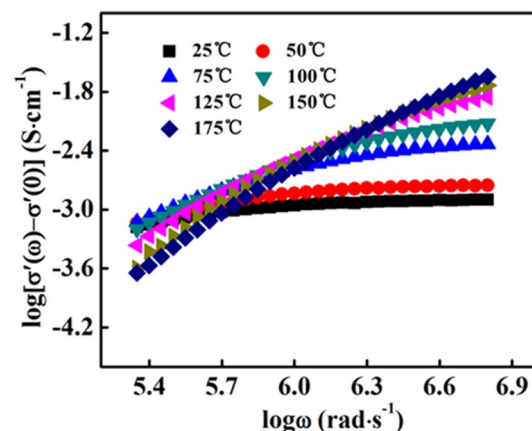
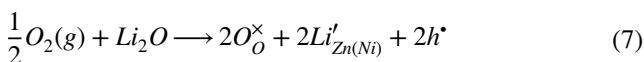


Fig. 8 Angular frequency ω dependence of the complex admittance $\sigma'(\omega)$ of the $(\text{Zn}_{0.3}\text{Ni}_{0.7})_{0.955}\text{Li}_{0.03}\text{Fe}_{0.015}\text{O}$ ceramic at different temperatures, $\log[\sigma'(\omega) - \sigma'(0)] - \log\omega$ plots

3.4 Conduction mechanisms

In the typical spinel manganite NTC ceramics, the conduction is generally believed to propagate by a polaron hopping model, in which the electron hopping takes place between the Mn^{3+} and Mn^{4+} cations locating at the octahedron B-sites [6, 7]. As discussed in the Eq. (6) and Fig. 8, the power exponents S are < 1 in the lower temperature region (≤ 125 °C), indicating that the electron-hopping conduction should be the conduction model for the $(\text{Zn}_{0.3}\text{Ni}_{0.7})_{1-x-y}\text{Li}_x\text{Fe}_y\text{O}$ conduction. For the hopping conduction, there must be valence-variable ions which have different valences locating at the same crystallographic sites. Generally, Ni-ion might have different valences for the arrangement of extra-nuclear electron of $3d^84s^2$, as discussed in Sect. 3.1, the XPS analysis confirms the existence of Ni^{2+} and Ni^{3+} . But Zn-ion, Li-ion do not have the variable valences. Therefore, the contribution to the hopping conduction mainly comes from the Ni-ions and the electron hopping between $\text{Ni}^{3+}\text{--Ni}^{2+}$ pairs can be expressed as $\text{Ni}^{3+} + \text{Ni}^{2+} \leftrightarrow \text{Ni}^{2+} + \text{Ni}^{3+}$. When the temperature increases, the thermal activation increases and enhances the electron hopping, resulting in the NTC effect.

On the other hand, both NiO and ZnO are semiconductors with the band gaps of 3.37 and 3.6–4.0 eV, respectively, the solid solutions of $\text{Zn}_{1-x}\text{Ni}_x\text{O}$ are also semiconductors and the related band gap changes with the Zn/Ni ionic ratio [33]. It is well known, Li-substitution into the $(\text{Zn}_{0.3}\text{Ni}_{0.7})_{1-x-y}\text{Li}_x\text{Fe}_y\text{O}$ lattice acts as the acceptor dopant and leading to the existence of conduction holes at the acceptor energy level, followed by the formation of p-type semiconductor. The related defect reaction can be written as Eq. (7).



As a result, the electron holes at the acceptor energy level can be activated to transport to the valence level and contribute the conduction in the $(\text{Zn}_{0.3}\text{Ni}_{0.7})_{1-x-y}\text{Li}_x\text{Fe}_y\text{O}$ ceramics, which follows the band conduction mechanism. As discussed in Eq. (6), the power exponents S are more than 1 at higher temperatures (≥ 150 °C), also confirms the existence of long range conduction, i.e., band conduction.

Because of the hopping conduction and the band conduction, the resistivity of grain (bulk) effect increase obviously with the temperature increases, indicating the NTC effect.

For the grain boundary effect, the grain-boundary barrier should be the main obstacle for the electron transport. Due to the complicate composition and structures at the grain boundaries, the related conduction mechanism should not simply conform the ones inside the grain. The charge carriers (electron and/or electronic hole) can transport between grains by overcoming the barrier by thermal activation. Assuming that the barrier energy is E_{gb} , the probability for a charge carrier reaching the E_{gb} is proportional to

$\exp(-E_{gb}/kT)$, according to the Boltzmann statistical distribution law. This indicates that the transport chance for the charge carrier overcoming the grain-boundary barrier increases is exponential relation with the temperature rise, i.e., the resistivity from the grain boundary effect also shows NTC characteristic induced by thermal activation.

4 Conclusions

The $(\text{Zn}_{0.3}\text{Ni}_{0.7})_{1-x-y}\text{Li}_x\text{Fe}_y\text{O}$ ceramics have a cubic phase with space group of $Fm\bar{3}m$ (225) as that of pure $\text{Zn}_{0.3}\text{Ni}_{0.7}\text{O}$. All the prepared $\text{Zn}_{0.3}\text{Ni}_{0.7}\text{O}$ -based ceramics show the typical NTC effect. The material-sensitivity constants and the room temperature resistivities can be effectively adjusted in a large range by changing the contents of Li- and Fe- ions, and can meet the wild requirements of the commercial applications. The conduction of $(\text{Zn}_{0.3}\text{Ni}_{0.7})_{1-x-y}\text{Li}_x\text{Fe}_y\text{O}$ ceramics results from both grain effect and grain-boundary effect. Hopping conduction and band conduction are proposed to be the conduction models for bulk conduction effect, while the thermal activation transport of charge carriers is proposed for the conduction model for grain boundary effect.

Acknowledgements The authors acknowledge the supports by the innovative project for graduate students of Central South University (No. 2017zzts661), the Laboratory Research Fund by the State Key Laboratory of Powder Metallurgy, China, and the National Nature Science Foundation of China (No. 51172287).

References

1. H. Gao, C. Ma, B. Sun, Preparation and characterization of NiMn_2O_4 negative temperature coefficient ceramics by solid-state coordination reaction. *J. Mater. Sci.* **25**, 3990–3995 (2014)
2. R.N. Jadhav, S.N. Mathad, V. Puri, Studies on the properties of $\text{Ni}_{0.6}\text{Cu}_{0.4}\text{Mn}_2\text{O}_4$ NTC ceramic due to Fe doping. *Ceram. Int.* **38**, 5181–5188 (2012)
3. F. Kenfack, H. Langbein, Spinel ferrites of the quaternary system Cu-Ni-Fe-O: synthesis and characterization. *J. Mater. Sci.* **41**, 3683–3693 (2006)
4. K. Xiong, S.X. Zhao, D.F. Li, Structure and electrical performance of $\text{Mn}_{1.5-0.5x}\text{Co}_{0.9-0.3x}\text{Ni}_{0.6-0.2x}\text{Cu}_x\text{O}_4$ NTC ceramics prepared by heterogeneous precipitation. *J. Alloys Compd.* **606**, 273–277 (2014)
5. K. Park, I.H. Han, Effect of Al_2O_3 addition on the microstructure and electrical properties of $(\text{Mn}_{0.37}\text{Ni}_{0.3}\text{Co}_{0.33-x}\text{Al}_x)\text{O}_4$ ($0 \leq x \leq 0.03$) NTC thermistors. *Mater. Sci. Eng. B* **119**, 55–60 (2005)
6. E.D. Macklen, Electrical conductivity and cation distribution in nickel manganite. *J. Phys. Chem. Solid* **47**, 1073–1079 (1986)
7. C. Ma, Y. Liu, Y. Lu, Preparation routes and electrical properties for $\text{Ni}_{0.6}\text{Mn}_{2.4}\text{O}_4$ NTC ceramics. *J. Mater. Sci.* **26**, 7238–7243 (2015)
8. J. Wu, Z. Huang, W. Zhou, C. Ouyang, Y. Hou, Investigation of cation distribution, electrical, magnetic properties and their correlation in $\text{Mn}_{2-x}\text{Co}_{2x}\text{Ni}_{1-x}\text{O}_4$ films. *J. Appl. Phys.* **115**, 113703 (2014)

9. A. Basu, A.W. Brinkman, R. Schmidt, Effect of oxygen partial pressure on the NTCR characteristics of sputtered $\text{Ni}_x\text{Mn}_{3-x}\text{O}_{4+6}$ thin films. *J. Euro. Ceram. Soc* **24**, 1247–1250 (2004)
10. A. Basu, A.W. Brinkman, T. Hashemi, NTC characteristics of bismuth based ceramic at high temperature. *Int. J. Inorg. Mater.* **3**, 1219–1221 (2001)
11. M.A.L. Nobre, S. Lanfredi, Negative temperature coefficient thermistor based on $\text{Bi}_3\text{Zn}_2\text{Sb}_3\text{O}_{14}$ ceramic: an oxide semiconductor at high temperature. *Appl. Phys. Lett.* **82**, 2284–2286 (2003)
12. M.A.L. Nobre, S. Lanfredi, Thermistor ceramic with negative temperature coefficient based on $\text{Zn}_7\text{Sb}_2\text{O}_{12}$: an inverse spinel-type phase. *Appl. Phys. Lett.* **81**, 451–453 (2002)
13. B. Yang, H. Zhang, J. Zhang, X. Zhang, Z. Li, Electrical properties and temperature sensitivity of B-substituted CuO-based ceramics for negative temperature coefficient thermistors. *J. Mater. Sci.* **26**, 10151–10158 (2015)
14. J. Zhang, H. Zhang, B. Yang, Y. Zhang, Z. Li, Temperature sensitivity of Fe-substituted SnO_2 -based ceramics as negative temperature coefficient thermistors. *J. Mater. Sci.* **27**, 4935–4942 (2016)
15. J. Wang, H. Zhang, X. Sun, Y. Liu, Z. Li, Electrical properties and temperature sensitivity of Li/Fe-modified NiO-based ceramics as NTC thermistors. *J. Mater. Sci.* **27**, 11902–11908 (2016)
16. G. Wang, H. Zhang, X. Sun, Y. Liu, Z. Li, Characterization of a new system of NTC temperature-sensitive ceramics based on Al/F modified NiO simple oxides. *J. Mater. Sci.* **28**, 363–370 (2017)
17. B. Yang, H. Zhang, J. Guo, Y. Liu, Z. Li, Electrical properties and thermal sensitivity of Ti/Y modified CuO-based ceramic thermistors. *Front. Mater. Sci.* **10**, 413–421 (2016)
18. J.A. Dirksen, K. Duval, T.A. Ring, NiO thin-film formaldehyde gas sensor. *Sens. Actuators B* **80**, 106–115 (2001)
19. C.C. Hu, H. Teng, Structural features of p-type semiconducting NiO as a co-catalyst for photocatalytic water splitting. *J. Catal.* **272**, 1–8 (2010)
20. X.H. Huang, J.P. Tu, C.Q. Zhang, Spherical NiO-C composite for anode material of lithium ion batteries. *Electrochim. Acta* **52**, 4177–4181 (2007)
21. F. Jiang, Z.J. Peng, Y.X. Zang, Progress on rare-earth doped ZnO-based varistor materials. *J. Adv. Ceram.* **2**, 201–212 (2013)
22. Y. Chen, P.I. Reyes, Z. Duan, Multifunctional ZnO-based thin-film bulk acoustic resonator for biosensors. *J. Electron. Mater.* **38**, 1605–1611 (2009)
23. Q. Pan, L. Qin, J. Liu, Flower-like ZnO-NiO-C films with high reversible capacity and rate capability for lithium-ion batteries. *Electrochim. Acta* **55**, 5780–5785 (2010)
24. G. Pei, W. Feng, C. Xia, Influences of Al doping concentration on structural, electrical and optical properties of $\text{Zn}_{0.95}\text{Ni}_{0.05}\text{O}$ powders. *Curr. Appl. Phys.* **8**, 18–23 (2008)
25. S.F. Shayesteh, R. Nosrati, The structural and magnetic properties of diluted magnetic semiconductor $\text{Zn}_{1-x}\text{Ni}_x\text{O}$ nanoparticles. *J. Supercond. Novel Magn.* **28**, 1–6 (2015)
26. X. Sun, H. Zhang, Y. Liu, J. Guo, Z. Li, Characterization of new negative temperature coefficient thermistors based on Zn-Ni-O system. *J. Adv. Ceram* **5**, 329–336 (2016)
27. B. Gokul, P. Saravanan, V.T.P. Vino, M. Černík, R. Sathyamoorthy, A study on the origin of room temperature ferromagnetism in $\text{Ni}_{1-x}\text{Gd}_x\text{O}$ nanoparticles. *J. Magn. Magn. Mater* **394**, 179–184 (2015)
28. Z. Guo, J. Shao, H. Lin, M. Jiang, S. Chen, Z. Li, Electrical conductivity & temperature sensitivity of ceramics based on NiO simple oxides for NTC applications. *J. Mater. Sci.* **28**, 11871–11877 (2017)
29. H. Von, R. Arthur, *Dielectrics and Waves*, 2nd edn. (Artech House Publishers, London, 1995)
30. A. Shukla, R.N.P. Choudhary, High-temperature impedance and modulus spectroscopy characterization of $\text{La}^{3+}/\text{Mn}^{4+}$ modified PbTiO_3 nanoceramics. *Curr. Appl. Phys.* **11**, 414–422 (2011)
31. P.G. Bruce, High and low frequency Jonscher behaviour of an ionically conducting glass. *Solid State Ionics* **15**, 247–251 (1985)
32. M.Z. Ansari, N. Khare, Thermally activated band conduction and variable range hopping conduction in $\text{Cu}_2\text{ZnSnS}_4$ thin films. *J. Appl. Phys.* **117**, 1 (2015)
33. W.B. Mi, H. Yang, Y.C. Cheng, Ferromagnetic half-metallic characteristic in bulk $\text{Ni}_{0.5}\text{M}_{0.5}\text{O}$ ($M = \text{Cu}, \text{Zn}$ and Cd): AGGA + U study. *Solid State Commun.* **152**, 1108–1111 (2012)